Journal of Science: Advanced Materials and Devices 5 (2020) 95–103

Contents lists available at ScienceDirect

Journal of Science: Advanced Materials and Devices

journal homepage: www.elsevier.com/locate/jsamd

Original Article

Epitaxial growth of Ce-doped $(Pb,Gd)_3(Al,Ga)_5O_{12}$ films and their optical and scintillation properties

Dmitrii A. Vasil'ev [a], Dmitry A. Spassky [b, c, *], Shunsuke Kurosawa [d, e], Sergey I. Omelkov [f], Natalia V. Vasil'eva [a], Victor G. Plotnichenko [g], Andrey V. Khakhalin [h], Valery V. Voronov [a], Vladimir V. Kochurikhin [a]

[a] Prokhorov General Physics Institute of the Russian Academy of Sciences, Vavilov Str., 38, 119991, Moscow, Russia
[b] National University of Science and Technology (MISIS), Leninskiy Prospect, 4, 119049, Moscow, Russia
[c] Skobeltsyn Institute of Nuclear Physics, Lomonosov Moscow State University, Leninskie Gory, 119991, Moscow, Russia
[d] New Industry Creation Hatchery Center, Tohoku University, Sendai, 980-8579, Japan
[e] Department of Physics, Yamagata University, Yamagata, 990-8560, Japan
[f] Institute of Physics, University of Tartu, W. Ostwald str. 1, 50411, Tartu, Estonia
[g] Fiber Optics Research Center, Russian Academy of Sciences, Vavilov Str., 38, 119333, Moscow, Russia
[h] Physics Department, Lomonosov Moscow State University, Leninskie Gory, 119991, Moscow, Russia

ARTICLE INFO

Article history:
Received 20 October 2019
Received in revised form
17 January 2020
Accepted 23 January 2020
Available online 31 January 2020

ABSTRACT

Ce-doped $(Pb,Gd)_3(Al,Ga)_5O_{12}$ single crystalline garnet films were grown using liquid-phase epitaxy from four series of supercooled $PbO-B_2O_3$-based melt solutions on $Gd_3Ga_5O_{12}$ and $Gd_3Al_{2.26}Ga_{2.74}O_{12}$ single crystal substrates. The optical and scintillation properties of the epitaxial garnet films were studied. The 5d-4f emission of Ce^{3+} ions within 450–650 nm was observed. The highest pulsed cathodoluminescence yield and scintillation yield values under ^{133}Ba excitation for the $Pb_{0.01}Ce_{0.02}Gd_{2.97}Al_{3.13}Ga_{1.87}O_{12}$ film were 43,100 photons/MeV and 20,000 photons/MeV, respectively. The pulsed cathodoluminescence decay times of the film were 1.8 (1%), 24 (25%), and 60 ns (74%), and the scintillation decay times were 3.9 (7%) and 43.6 ns (93%). Because of the rapid decay and high light yield, Ce-doped $(Pb,Gd)_3(Al,Ga)_5O_{12}$ garnet films can be used in X-ray scintillators for different applications, such as homeland security.

1. Introduction

Epitaxial films grown via liquid-phase epitaxy (LPE) have been used as scintillation detectors for high-resolution micro-imaging, stimulated scintillation emission depletion X-ray imaging and electron detection in scanning electron microscopy. Lu_2SiO_5:Tb epitaxial films have the best prospects for imaging applications [1–3], while $Gd_3Al_{5-x}Ga_xO_{12}$:Ce (GAGG:Ce) films can be used in scanning electron microscopy [4]. The rapid scintillation decay time is an advantage of Ce-doped garnet films. The fast decay of GAGG:Ce can be further improved by increasing the Ga concentration. However, for GAGG:Ce single crystals, increasing the Ga concentration by $x > 2$ decreases the light yield [5]. Similar adverse effect can be expected for single crystalline films. Co-doping of GAGG:Ce crystals with divalent ions such as Ca or Mg [6–9] also improves the time characteristics. This changes the valency of the cerium ions from 3+ to 4+ and accelerates the energy transfer process to the emission centres. Single crystalline garnet films can be grown from supercooled $PbO-B_2O_3$-based [10,11] and $Bi_2O_3-B_2O_3$-based [12–14] melt solutions. During the epitaxial process, the film captures solvent impurities from the melt: Pb^{2+} ions and Pb^{2+}-Pb^{4+} pairs or Bi^{3+} ions. The impurity ions in the epitaxial films cause additional absorption bands, likely affecting the valence state of the cerium ions. In particular, Pb^{2+} ions are non-isovalent impurities in the garnet structure that promote the formation of Ce^{4+} centres [8,15,16].

This study reports the optical and scintillation properties of $(Pb,Gd)_3(Al,Ga)_5O_{12}$:Ce films grown via LPE from supercooled $PbO-B_2O_3$-based melt solutions.

2. Experimental

2.1. Growth of epitaxial films

Ce-doped $(Pb,Gd)_3(Al,Ga)_5O_{12}$ garnet films were grown using a platinum crucible on (111)-oriented single crystal $Gd_3Ga_5O_{12}$ (GGG) substrates with a lattice parameter (a_s) of 12.383 Å or

* Corresponding author. National University of Science and Technology (MISIS), Leninskiy Prospect, 4, 119049 Moscow, Russia.
E-mail address: daspassky@gmail.com (D.A. Spassky).
Peer review under responsibility of Vietnam National University, Hanoi.

https://doi.org/10.1016/j.jsamd.2020.01.005

12.376 Å and on (320)-oriented single crystal $Gd_3Al_{2.26}Ga_{2.74}O_{12}$ (GAGG) substrates (a_s = 12.255 Å) via LPE from supercooled high-temperature PbO–B_2O_3-based melt solutions with gadolinium oxide $C(Gd_2O_3)$ concentrations between 0.2 and 0.5 mol%, $C(CeO_2)$ concentrations of 0.2 and 0.3 mol%, and $C(Al_2O_3)$ concentrations of 4.5 mol% in the mixture (Table 1). Starting materials Gd2O3, CeO_2, Al_2O_3, Ga_2O_3, and PbO and B_2O_3 powders of 4 N~5 N purity were used. The melt solution was homogenised in the platinum crucible for at least 4 h. The temperature of the melt solution was reduced stepwise to the growth temperature (T_g). For each step, the substrate, secured to a platinum holder, was immersed in the melt solution in a horizontal position for 5 min. When the melt solution temperature was higher than the equilibrium crystallisation temperature or saturation temperature (T_{sat}), the substrate dissolved. When the melt solution temperature was below the T_{sat}, a film grew on both sides of the substrate at a constant temperature. The rotation speed of the substrate during the film growth was 50 or 132 rpm. The film growth times were 5–360 min.

2.2. Experimental methods

The quantitative chemical analysis of the grown films was performed and SEM images of the selected films and spontaneously grown garnet single crystal were obtained with a Quanta 3 D FEG electron-ion scanning microscope. The error margins of the composition were 0.01 formula units for Pb and Ce ions.

The total thickness (2 h) of the films grown on both sides of the substrate was ascertained by weighing the substrate prior to and after epitaxial growth. The differences in the densities of the grown film and substrate were neglected.

The films were characterised by X-ray diffraction using a Bruker D8 Discover A25 Da Vinci Design X-ray diffractometer (CuKα radiation).

To simplify the spectroscopic studies, we did not remove the films from the back side of the substrate. The transmission spectra of the films were measured using a PerkinElmer Lambda 900 spectrophotometer in a 250–550 nm wavelength range at room temperature. The optical density D was derived from the transmission using the formula $D = [\ln (T_s/T_{fsf})]$, where T_s is the transmission spectrum of the substrate and T_{fsf} is the transmission spectrum of the substrate with grown films on both sides. To analyse the absorption spectra of the films, we used the normalised optical density D/2h to compare the intensity of the absorption bands of the films with different thicknesses.

The photoluminescence spectra of the films were measured at 300 K in the 400–700 nm region at E_{ex} = 165 nm (7.5 eV) under excitation by a Heraeus D 200 VUV deuterium lamp with a McPherson Model 234/302 primary monochromator. An Andor Shamrock 303i secondary monochromator with a Hamamatsu H8259 photomultiplier tube (PMT) was used as the detection system.

The excitation spectra were obtained at 300 K in the 200–500 nm region at E_{lum} = 540 nm (2.29 eV) under excitation by a 150 W xenon lamp with an MDR-206 primary monochromator. The temperature dependence of the Ce^{3+} emission intensity was measured in the 100–500 K region at E_{ex} = 450 nm (2.76 eV). The measurements were obtained using a vacuum optical Cryotrade LN-120 cryostat equipped with a Lake Shore 335 temperature controller at a heating rate of 20 K/min. The luminescence was detected using an Oriel MS257 spectrograph equipped with a Marconi CCD detector.

The radioluminescence spectra excited by 5.5-MeV alpha particles from a ^{241}Am source were measured on an FLS920 spectrofluorometer (Edinburgh Instruments) at room temperature.

Table 1
Composition of the melt solutions and growth parameters for Ce $(Pb,Gd)_3(Al,Ga)_5O_{12}$ Epitaxial films.

Series number	$C(Gd_2O_3)$ (mol %)	$C(CeO_2)$ (mol %)	$C(Al_2O_3)$ (mol %)	Temperature rang (δT, °C)	Supercooling degree (ΔT, °C) min–max	Thickness h_{max} (μm)	Growth rate f_{max} (μm/min)	Film num-ber	Film composition/substrate	Supercooling degree (ΔT, °C)	Thickness h (μm)
I	0.2	0.2	0	987–966	4–82	10.8	0.30	I-1	$Pb_{0.02}Ce_{0.03}Gd_{2.95}Ga_5O_{12}$/GGG	33	3.7
II	0.4	0.2	4.5	1093–1065	17–76	90.8	1.44	II-1	$Pb_{0.01}Ce_{0.03}Gd_{2.96}Al_{3.14}Ga_{1.86}O_{12}$/GGG	22	14.3
								II-2	$Pb_{0.01}Ce_{0.02}Gd_{2.97}Al_{3.13}Ga_{1.87}O_{12}$/GGG	20	43.3
								II-3	$Pb_{0.01}Ce_{0.06}Gd_{2.93}Al_{3.14}Ga_{1.86}O_{12}$/GGG	44	90.8
								II-4	$Pb_{0.01}Ce_{0.02}Gd_{2.97}Al_{3.14}Ga_{1.86}O_{12}$/GAGG	42	22.4
								II-5	$Pb_{0.01}Ce_{0.04}Gd_{2.95}Al_{3.14}Ga_{1.86}O_{12}$/GGG	20	14.5
								II-6	$Pb_{0.01}Ce_{0.04}Gd_{2.95}Al_{3.14}Ga_{1.86}O_{12}$/GGG	29	26.5
								II-7	$Pb_{0.01}Ce_{0.03}Gd_{2.96}Al_{3.14}Ga_{1.86}O_{12}$/GGG	17	61.4
III	0.4	0.3	4.5	1075–1065	5–25	91.5	0.80	III-1	$Pb_{0.01}Ce_{0.04}Gd_{2.95}Al_{3.14}Ga_{1.86}O_{12}$/GGG	18	91.5
IV	0.5	0.2	4.5	1083–1076	4–45	73.0	1.22	IV-1	$Pb_{0.01}Ce_{0.03}Gd_{2.96}Al_{3.13}Ga_{1.87}O_{12}$/GGG	45	50.7

The pulse height spectra were recorded using an R7600U-200 PMT (Hamamatsu Co). The PMT signal was amplified and shaped with a shaping time of 2 μsec using a shaping amplifier (ORTEC 752A) and registered with an MCA 8000A multichannel analyser. The spectra were registered using a ^{133} Ba radioactive source.

The pulsed cathodoluminescence (PCL) spectra and decay curves were recorded using a pulsed cathodoluminescence setup based on a Radan-303A electron gun [17]. An electron beam with a broad spectrum and E_{max}~120 keV, FWHM pulse of 200 ps, and peak electron current of 10 A/cm^2 was used as the excitation. An Andor iStar iCCD was used to obtain the gated spectra in a 0–2 ms time window. The spectra were corrected by the system's spectral sensitivity. For the decay curves, a Hamamatsu R3809U-50 MCP-PMT was used in the pulse current mode with a response of 250 ps FWHM. The thickness of the films >40 μm provided full absorption of the electron beam.

The scintillation decay curves under excitation by ^{57}Co (122 keV) were measured using the Hamamatsu R7600U-200 PMT connected to a Tektronix TDS3034B oscilloscope.

3. Results and discussion

3.1. Growth of Ce:(Pb,Gd)$_3$(Al,Ga)$_5$O$_{12}$ films

Ce-doped (Pb,Gd)$_3$(Al,Ga)$_5$O$_{12}$ garnet films were grown by LPE. A total of 32 10 × 15 mm^2 samples (film-substrate-film) were grown from four series of PbO–B_2O_3 melt solutions. All of the grown films were yellow-green. An image of some of the films and substrate under 405 nm excitation is shown in Fig. 1. The (Pb,Gd)$_3$(Al,Ga)$_5$O$_{12}$:Ce films had Ce^{3+}-related yellow-green luminescence, while the weak red luminescence of the (Pb,Gd)$_3$Ga$_5$O$_{12}$:Ce film and $Gd_3Ga_5O_{12}$ substrate was likely due to accidental impurities. The temperature range δT, including the saturation temperature (T_{sat}) and supercooling degree $\Delta T = T_{sat} - T_g$, was determined for all of the investigated melt solutions (see Table 1). The maximum thickness of the grown epitaxial films (h_{max}) and highest growth rate (f_{max}) were also determined for each series. The maximum thickness was obtained for the epitaxial films that were grown from the II and III melt solutions. SEM images of films II-2 and IV-1 are presented in Fig. 2. The surface of the IV-1 film was rather smooth whereas that of film II-2 was rough with bulges. The X-ray diffraction patterns obtained in the θ/2θ scanning mode showed only strong 444 and 888 reflections from the films grown from the II melt solution and weak 444 and 888 reflections from its substrates shielded by the films. Diffraction patterns were recorded on both sides of the samples. The maxima positions of the peaks differed by less than 0.005°. From the peak positions, we determined the lattice parameters of the GGG substrates, a_s = 12.376 Å and 12.3829 Å. The lattice parameters of the substrates agreed with JCPDS Powder Diffraction File data for GGG (card nos. 00-013-0493 and 01-071-0701). In films of different thicknesses, the maxima positions differed markedly. The lattice parameter (a_f) decreased as the film thickness increased. The lattice parameter for film II-5 (h = 14.5 μm) was 12.219 Å, for film II-6 (h = 26.5 μm) was 12.214 Å, and for film II-7 (h = 61.4 μm) was 12.206 Å. The relative lattice mismatch $\Delta a = (a_s - a_f)/a_f$ x 100% was 1.3% for film II-6. This means that to obtain films of high crystallographic quality, it is necessary to grow them on substrates with a lattice parameter of less than 12.376 Å, for example, on GAGG substrates with 12.255 Å for which the relative mismatch is less than 1%. The correspondence of the crystallographic directions of filmII-6 and substrate GGG was determined by recording the ϕ scanning of asymmetric reflections 880 and 12.60 for the film and substrate (Fig. 3). The diffraction patterns demonstrate that those films were single crystalline and epitaxially superimposed on the substrate. The high background on the substrate diffraction patterns was explained by the fluorescence of the gadolinium in the detector's sensitivity window.

Spontaneous crystallisation occurred in the bulk of the melt solution simultaneously with the film growth. This caused the appearance of garnet single crystals in the shape of tetragon-trioctahedrons with {2 1 1} faces (Fig. 4).

3.2. Optical absorption

The normalised optical density spectra are presented in Fig. 5. The absorption band at 282 nm (4.4 eV) in film I-1 was due to the $(6s^2)\ ^1S_0 \rightarrow\ ^3P_1$ electronic transition in the Pb^{2+} ions (Fig. 5a) according to [18]. The absorption bands related to Gd^{3+} were absent in the spectra of the films because these bands were divided out during the mathematical calculation of the spectra (see Section Experimental methods for details). When Al was introduced into the mixture of film II-1, the band maximum shifted to 273 nm (4.54 eV), that is by 9 nm to shorter wavelengths. Two other broad absorption bands corresponded to the 4f ($^2F_{5/2,7/2}$) → 5d electronic transition of the Ce^{3+} ions. The absorption band maximum of the $5d_1$ level clearly shifted from 426 (2.91 eV) to 444 nm (2.79 eV), that is, by 18 nm to longer

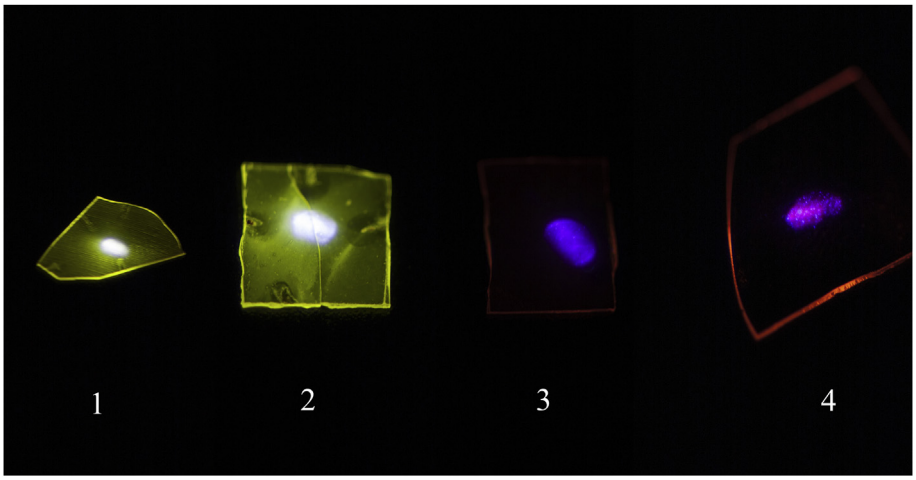

Fig. 1. Photo of film II-4 (1), film II-2 (2), film I-1 (3), and $Gd_3Ga_5O_{12}$ substrate (4) at E_{ex} = 3.06 eV (405 nm); the numbers identify the films as referenced in Table 1.

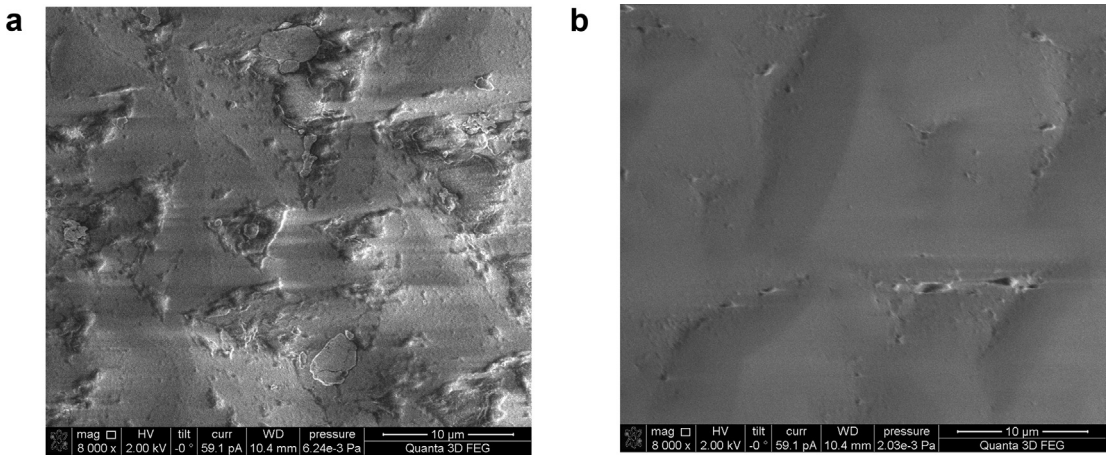

Fig. 2. Electron images of surface of $Pb_{0.01}Ce_{0.02}Gd_{2.97}Al_{3.13}Ga_{1.87}O_{12}$ film II-2 (a) and $Pb_{0.01}Ce_{0.03}Gd_{2.96}Al_{3.13}Ga_{1.87}O_{12}$ film IV-1 (b) (see Table 1 for details).

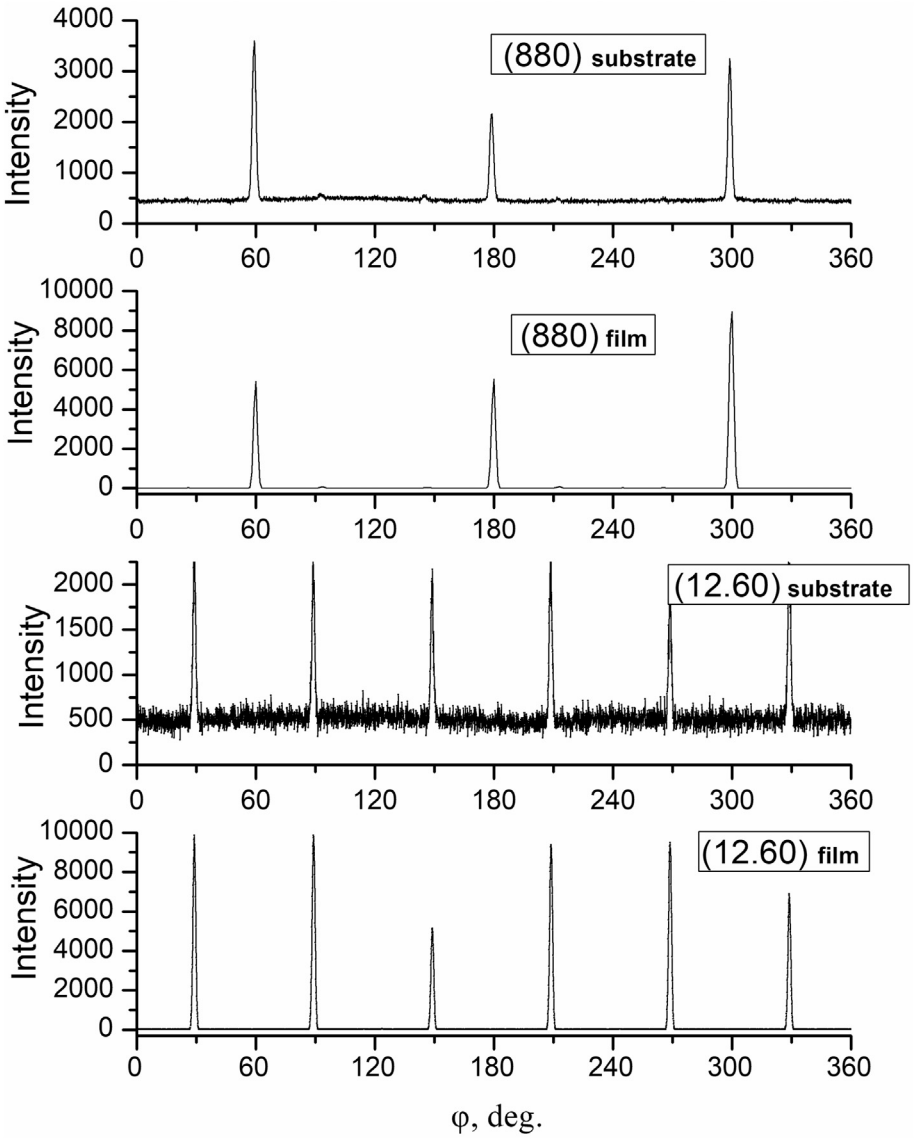

Fig. 3. Asymmetric 880 and 12.60 reflections obtained via azimuthal scanning of the GGG substrate and film II-6.

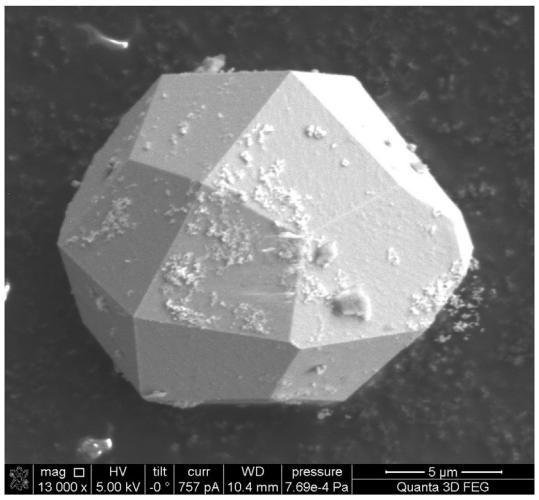

Fig. 4. Microphotography of spontaneously grown garnet single crystal of $Pb_{0.01}Ce_{0.15}Gd_{2.84}Al_{3.74}Ga_{1.26}O_{12}$ composition grown from the II melt solutions series made by a scanning electron microscope.

wavelengths, and the band maximum of the $5d_2$ level shifted from 346 (3.58 eV) to 340 nm (3.65 eV), that is, by 6 nm to shorter wavelengths (Fig. 5a, curves 2 and 3). The shift of the Ce-related absorption bands in the grown films agreed well with the trend observed in $Gd_3Al_xGa_{5-x}O_{12}$:Ce scintillators and was due to an increase in the crystal field strength and band gap value as the Al content increased [19]. The narrow absorption bands in the wavelength ranges from 250 to 255 nm, 272–280 nm, and 302–314 nm in the GGG substrate spectrum (Fig. 5a, curve 1) corresponded to the (4f7) $^8S_{7/2} \rightarrow {}^6D$, $^8S_{7/2} \rightarrow {}^6I$, and $^8S_{7/2} \rightarrow {}^6P$ electronic transitions in the Gd^{3+} ions, respectively [11,20]. Fig. 5b shows the normalised optical density spectra of the films grown from the II, III, and IV melt solution series, and the curve numbers identify the films referenced in Tables 1 and 2. The thickness of these films was higher than presented in Fig. 5a. For these films, only the Ce-related bands were observed, while at $\lambda < 310$ nm, the films were opaque. In particular, the spectra show the 4f-$5d_1$ absorption band of the Ce^{3+}, and the intensity depended on the Ce concentration (Fig. 5b, curves 1–3). The higher rate of absorption in the II-2 film in the transparency region was related to its rough surface (Fig. 2). The incident light scattered at the surface inhomogeneities, which resulted in a decrease in the transparency.

Fig. 6 shows the absorption spectra of the films from the II and IV series with similar Ce concentrations. The curves were obtained from the spectra of the normalised optical density by subtracting the constant component, which enabled a comparison of the absorption band intensities of the Ce^{3+} ions without the influence of the optical quality. The optical absorption of the grown films increased in the region below 360 nm in the films grown from the IV melt solution as the intensity of the $5d_1$ absorption band decreased.

3.3. Luminescence and scintillation characteristics

The photoluminescence spectra of the $Ce(Pb,Gd)_3(Al,Ga)_5O_{12}$ films were characterised by a broad non-elementary band peaking at 532 nm (2.33 eV), which corresponded to the radiative 5d-4f transition in the Ce^{3+} ions as shown in films II-2, III-1, and IV-1 in Fig. 7a. Ce^{3+} emission was not observed in the I-1 film because the 5d levels of the Ce^{3+} were enveloped by the conduction band states when Al was not introduced into the film composition [19]. The films grown from the III and IV melt solutions had decreased photoluminescence intensity relative to II-2. All of the films had similar Al/Ga ratios but substantially different concentrations of Ce ions (from 0.02 to 0.06). However, there was no direct correlation between the luminescence intensity of the films and the concentration of the Ce^{3+} ions. We suppose that the intensity of the films was determined by their synthesis features (the growth rate and supercooling degree).

Four pronounced bands appeared in the excitation spectra of films IV-1 and II-2. The bands at 448 nm (2.77 eV) and 343 nm (3.61 eV) were ascribed to electron transitions from the 4f to $5d_1$ and $5d_2$ states of the Ce^{3+} ions. The band at 278 nm (4.46 eV) was a superposition of two bands related to $^1S_0 \rightarrow {}^3P_1$ and $^8S_{7/2} \rightarrow {}^6I$ in the Pb^{2+} and Gd^{3+} ions, respectively. The latter indicates the energy transfer from the Gd^{3+} and/or Pb^{2+} ions to the Ce^{3+} ions. Weak excitation bands were also detected at 308 and 314 nm, which were attributed to $^8S_{7/2} \rightarrow {}^6P$ electronic transitions in the Gd^{3+} ions. The non-elementary broad band peaking at 215 nm (5.77 eV) was ascribed to the superposition of several bands related to the 4f-$5d_{3\text{-}5}$ transitions in the Ce^{3+} with a defect-related band and, probably, charge–transfer transitions involving the Ce^{4+} ions.

The temperature dependence of the Ce^{3+} emission intensity of film II-2 is presented in Fig. 7b. The emission was partially quenched (by 25%) at 300 K relative to the maximum observed in the 100–150 K region. Quenching occurred in several stages and could not be approximated using a simple Mott formula [21]. The

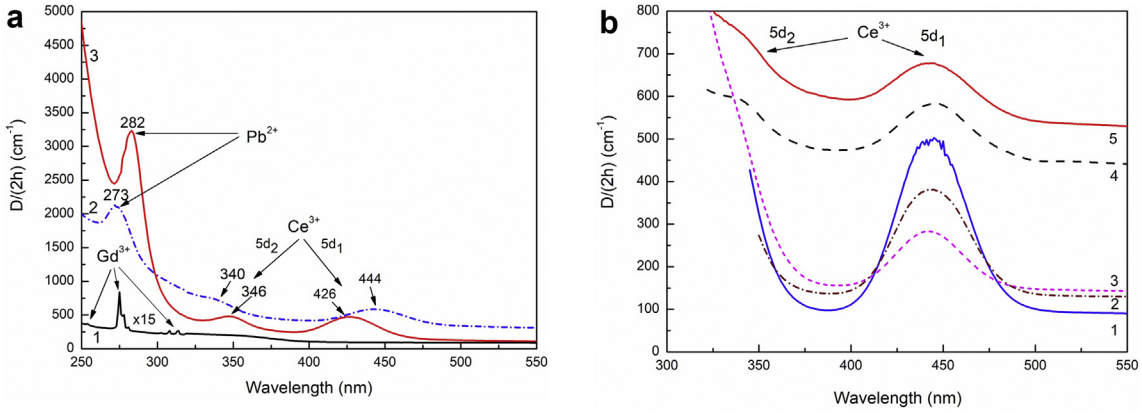

Fig. 5. Normalized optical density spectra of (a) $Gd_3Ga_5O_{12}$ substrate, h = 460 µm (1); film II-1, h = 14.3 µm (2); film I-1, h = 3.7 µm (3), and (b) film II-3, h = 90.8 µm (1); film III-1, h = 91.5 µm (2); film IV-1, h = 50.7 µm (3); film II-4, h = 22.4 µm (4); film II-2, h = 43.3 µm (5); the numbers identify the films as referenced in Tables 1 and 2.

Table 2
Decay time and light output of $Ce(Pb,Gd)_3(Al,Ga)_5O_{12}$ Epitaxial films.

Film number	PCL Yield, (% of LYSO)	PCL Yield, (ph/MeV)	Scintillation light yield @662 keV, (ph/MeV)[b]	Scintillation light yield @^{133}Ba (ph/MeV)	Degree of yield proportionality[c]	PCL decay time τ_1 (ns)	PCL decay time τ_2 (ns)	PCL decay time τ_3 (ns)	Scintillation decay time τ_1 (ns)	Scintillation decay time τ_2 (ns)
II-2	181	43,100	45,300	~20,000	46%	1.8 (1%)	24 (25%)	60 (74%)	3.9 (7%)	43.6 (93%)
II-3	129	30,700	32,300	~18,000	58%	2.0 (2%)	24 (29%)	59 (69%)	14.8 (14%)	49.6 (86%)
III-1	95	22,600	23,800	~11,000	48%	1.9 (2%)	21 (28%)	55 (70%)	2.9 (3%)	42 (97%)
IV-1	23	5500	5800	~4000	72%	1.2 (7%)	8.4 (32%)	33 (61%)	5.8 (42%)	27.83 (58%)
Typical GAGG:Ce Bulk crystal	N.D.[a]	N.D.	~56,500 [30]	N.D.	~85% [30]	N.D.	N.D.	N.D.	70–100	N.D.
Typical LYSO:Ce Bulk crystal	100	23,800	28,000 [26]	N.D.	N.D.	N.D.	N.D.	N.D.	N.D.	N.D.
Typical CeF_3 Bulk crystal	15	3600	4500 [27]	N.D.	N.D.	N.D.	N.D.	N.D.	N.D.	N.D.

[a] N.D. (Not detected).
[b] For the films, scintillation light yield @662 keV is a hyopthetical value calculated from the PCL yield assuming full absorption of gamma quantum and nonproportionality at 100 keV as 95%.
[c] Degree of proportionality = Scintillation light yield@^{133}Ba divided by PCL light yield.

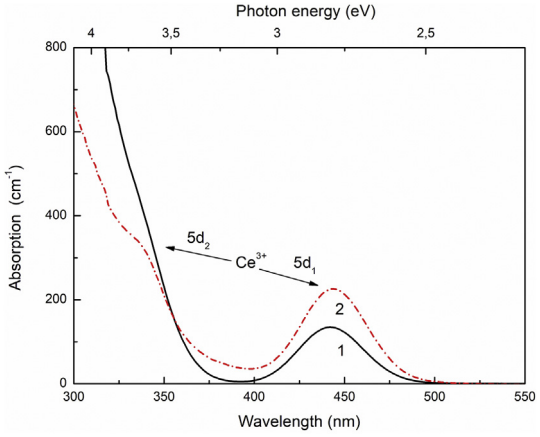

Fig. 6. Absorption spectra of films IV-1 (1) and II-1 (2) (see Table 1).

450 nm excitation wavelength corresponded to the intracentre 4f-$5d_1$ transitions in the Ce^{3+} ions. It was recently reported for Ce-doped garnets that the thermal quenching of Ce^{3+} emission is related to the thermal ionisation of electrons to the conduction band [22]. The quenching mechanism in the $Ce(Pb,Gd)_3(Al,Ga)_5O_{12}$ films was likely related to the thermal ionisation of the electrons from $5d_1$ Ce^{3+} to the conduction band and/or the electron states of the nearby defects.

The normalised radioluminescence spectra of films IV-1 and II-2 are presented in Fig. 8. The films had broad emission bands peaking at 560 nm (2.17 eV) that corresponded to the radiative 5d-4f transition within the Ce^{3+} ions.

The pulse height spectra of the films were obtained using the radioactive ^{133}Ba source and are presented in Fig. 9. The absolute value of the scintillation light yield was obtained using as reference sample a GSO:Ce single crystal with a known light yield. The data on the light yield and other scintillation parameters of the studied films and reference crystals are shown in Table 2. The II series film had the highest light yield values (Fig. 9).

Fig. 10 shows the pulse cathodoluminescence (PCL) spectra of several films compared with standard scintillation materials LYSO:Ce and CeF_3. Generally, the dependence of the scintillation light yield obtained from the pulse height spectra was similar to the dependence of the luminescence intensity presented in Fig. 10. There also was no direct dependence on the Ce^{3+} concentration. Films II-2 and II-3 had similar scintillation yield values while the concentration of the Ce ions in II-3 was three times higher than in II-2. Therefore, the scintillation yield was mainly determined by the growth features of the films. The presented spectra were corrected for the spectral sensitivity of the detection system, which enabled us to calculate the PCL yields of the different films using a method that was successfully applied in [23]. We used the yields measured at 662 keV gamma excitation for LYSO:Ce (28,000 photons/MeV [24]) and CeF_3 (4500 photons/MeV [25]) and corrected them using non-proportionality data [26,27] to obtain the yield at 100 keV (the median electron beam energy). The resulting PCL yield values relative to standard samples are included in Table 2. The PCL yield values were significantly higher than the scintillation yield values obtained using the ^{133}Ba radioactive source due to different reasons. One factor may have been the non-proportionality of the yield with respect to the energy of the exciting quantum, which led to a decrease in the yield under low-energy photons (such as those emitted by ^{133}Ba) with

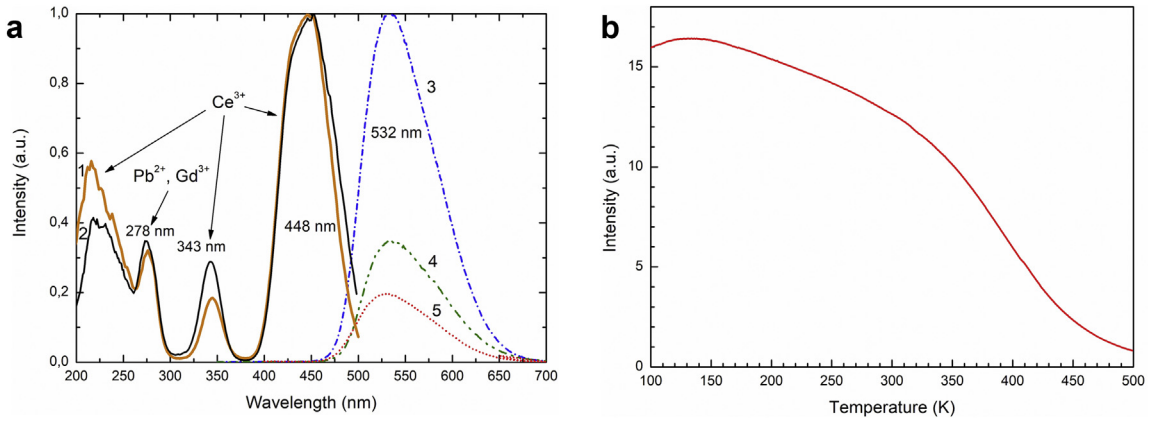

Fig. 7. Photoluminescence spectra of films II-2 (3); III-1 (4), IV-1 (5) at E_{ex} = 165 nm (7.5 eV), T = 300 K and photoluminescence excitation spectrum of films IV-1 (1), II-2 (2) at E_{em} = 540 nm (2.29 eV), T = 300 K (a). Temperature dependence of Ce^{3+} emission intensity of film II-2 in the 100–500 K region at E_{ex} = 450 nm (2.76 eV) (b).

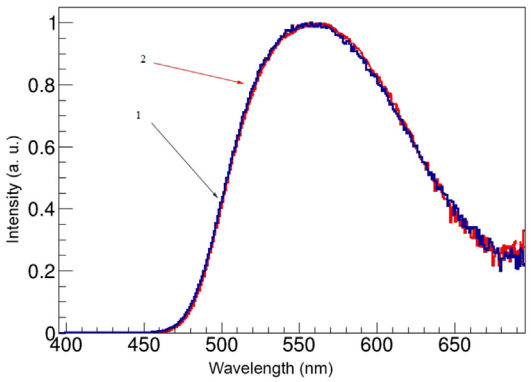

Fig. 8. Normalized radioluminescence spectra of films: IV-1 (1); II-2 (2).

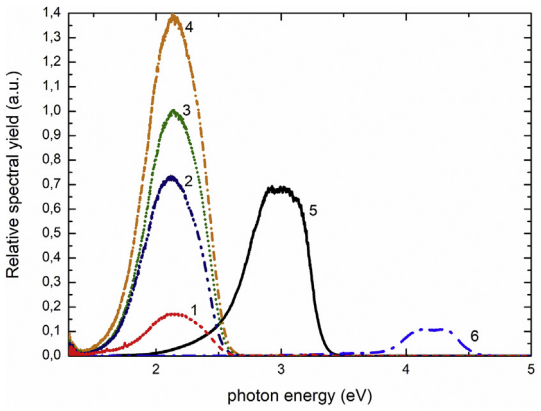

Fig. 10. The pulsed cathodoluminescence spectra of films IV-1 (1); III-1 (2); II-3 (3)); II-2 (4) and standard scintillation materials: LYSO:Ce (5) and CeF_3 (6), recorded in a time window from 0 to 2 ms relative to the excitation pulse. Curves are corrected to the spectral sensitivity of the system.

respect to the yield at 662 keV in the same scintillator, which was 100%. A detailed study [28] reported that at 100 keV, the yield of GAGG:Ce was approximately 90–95%, and at lower energies, the yield proportionality strongly depended on the Al:Ga ratio. At a classical ratio of 2.0:3.0, the yield at 30 keV was 85%, but increasing the Al content to 2.6:2.4 increased the yield at 30 keV to 95%. However, it was unclear how high the yield proportionality was in our films grown from the II, III, and IV melt solution series, as the Al:Ga ratio was even higher (3.14:1.86). Table 2 shows the degree of proportionality of the films, which was calculated as ratio of the scintillation yield (obtained using the ^{133}Ba source) to the PCL yield. These values were clearly lower than 95% measured for the bulk crystal with a 2.6:2.4 Al:Ga ratio. In addition to the intrinsic non-proportionality, these values could in part be explained by geometry: the electrons were always fully absorbed in the film, while the attenuation length of a 30 keV X-ray photon in GAGG was over 150 μm [29], making full absorption less likely. Film II-3 grown from the same melt solution as II-2 had a significantly higher degree of proportionality (58% vs 46%), which might have been because it was twice as thick. The same trend, however, did not occur when comparing the films grown from different melt solutions.

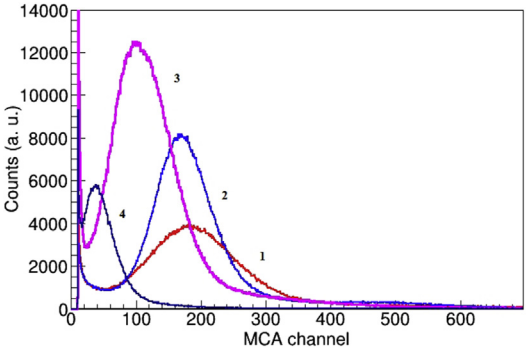

Fig. 9. Pulse height spectra of films: II-2 (1); II-3 (2); III-1 (3); IV-1 (4).

Using the PCL yield values and GAGG:Ce non-proportionality at 100 keV as 95% [28], we estimated the hypothetical yield of the film material at 662 keV gamma excitation. A bulk crystal of the same structure and composition would fully absorb such gamma quantum. Although these values do not characterise the films themselves, they are useful to compare the films to a bulk GAGG:Ce scintillator. Film II-2 with the highest scintillation yield @662 keV of 45,300 photons/MeV was already 80% of the bulk crystal yield; therefore, further improvements in the film composition and growth parameters will only slightly enhance the yield.

The PCL and scintillation decay curves of film II-2 are presented in Fig. 11. Three (PCL) and two (scintillation) decay components

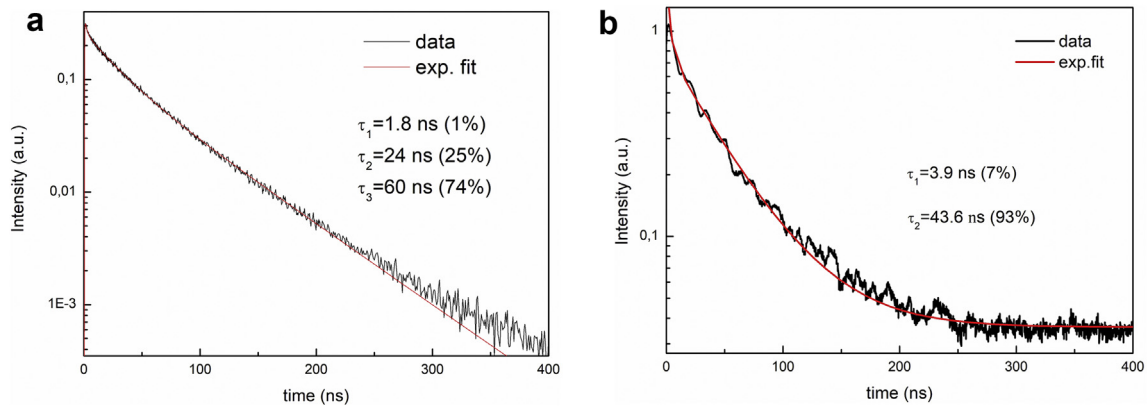

Fig. 11. (a) PCL decay curve and (b) scintillation decay curve of film II-2, recorded at 550 nm (2.25 eV). Curve (b) was measured under the excitation from ^{57}Co (122 keV).

were used to describe them. The decay times and their relative intensities were 1.8 (1%), 24 (25%), and 60 ns (74%) for the PCL decay curve and 3.9 (7%) and 43.6 ns (93%) for the scintillation decay curve. The decay curves of all of the samples were shorter under the ^{133}Ba source excitation (Table 2). In general, Ce decay in oxide scintillators tends to decrease when the density of the secondary low-energy excitations increases. This was directly demonstrated in YAG:Ce with VUV radiation that emulates secondary excitations [30]. As the primary excitation energy decreases from 100 to ~30 keV, the number of regions with high-density secondary excitations in the particle track increases [31], which is the primary cause of both decay shortening and yield non-proportionality.

Our experiments showed that the film IV-1 is characterised be the shortest decay times as well as the lowest light yield (Table 2). This may be connected with the presence of Ce^{4+} ions in the film. Recently it was shown that the presence of Ce^{4+} in GAGG single crystals results in light yield decrease [32] and in suppression of slow decay components [8]. It is worth noting that this film has other distinctive features, which also indicate the presence of Ce^{4+} ions. The increased optical absorption in the region below 360 nm can be ascribed to the electron charge–transfer transition from the top of the valence band (formed by the O^{2-} levels) to the Ce^{4+} ground state [6,33]. In LYSO:Ce,Ca^{2+} and LYSO:Ce,Mg^{2+} single crystals, similar increased absorption in the region up to 325 nm and decreased absorption in the $5d_1$ band were also explained by the formation of Ce^{4+} [34]. The increased of excitation peak intensity at 230 nm (Fig. 7a) may be also connected with the contribution of charge–transfer transitions between the oxygen 2p orbitals of the valence band and the Ce^{4+} 4f orbitals. The higher concentration of Ce^{4+} ions in the IV-1 film can be tentatively related to the higher concentration of Pb^{2+} ions in the film that promotes the formation of Ce^{4+} centres [8,15,16]. The distinctive feature of this film was the highest supercooling degree ΔT, which may result in a higher probability of the capture of solvent components into the film. However, the determined Pb content in the films was at the level of error margins and does not allow to reveal the change of Pb content from film to film.

The scintillation light yield of film II-4 was also measured under excitation by 5.5 MeV alpha particles from ^{241}Am as 18–21% of the bulk GAGG:Ce. Under excitation by 662 keV photons from ^{137}Cs, film II-4 had scintillation decay times and partial intensities of 28 ns (~74%) and 81 ns (~16%), respectively. Although the decay times of film II-2 depended slightly on the excitation type, the longest component was below 100 ns, characterising this film as a rapid scintillator, which can be used in X-ray scintillators for different applications.

4. Conclusion

Ce-doped $(Pb,Gd)_3(Al,Ga)_5O_{12}$ single crystalline garnet films were grown via LPE from supercooled $PbO–B_2O_3$-based melt solutions. The chemical compositions and lattice parameters of the films were determined. The introduction of Al^{3+} ions into the films' composition shifts the absorption band maxima of the Pb^{2+} and Ce^{3+} ions that is due to the increase of the crystal field strength. The broad emission band at 450–650 nm was observed and related to 5d-4f emission of Ce^{3+} ions. The luminescence excitation spectra demonstrate energy transfer from the Gd^{3+} and/or Pb^{2+} ions to the Ce^{3+} ions. It was supposed that Ce^{4+} centres are formed in the films grown from the melt solutions with $C(Gd_2O_3) = 0.5$ mol%, $C(CeO2) = 0.2$ mol%, and $C(Al2O3) = 4.5$ mol% in the mixture. The presence of Ce^{4+} was indicated by an intensity decrease in the Ce^{3+} absorption bands with a simultaneous increase in the absorption at $\lambda < 310$ nm, an increase in the excitation peak intensity at 230 nm, and a decrease in both the light yield and scintillation decay times. The highest PCL (43,100 photons/MeV) and scintillation (20,000 photons/MeV) light yields occurred in the films grown from the melt solutions with $C(Gd_2O_3) = 0.4$ mol%, $C(CeO_2) = 0.2$ mol%, and $C(Al_2O_3) = 4.5$ mol%. Thus, Ce-doped $(Pb,Gd)_3(Al,Ga)_5O_{12}$ garnet films can be used in X-ray scintillators for different applications, such as homeland security, because of their rapid decay and high light yield.

Declaration of interests

The authors declare that they have no known competing financial interests or personal relationships that could have appeared to influence the work reported in this paper.

Acknowledgements

The work was carried out with financial support from the Ministry of Science and High Education of the Russian Federation in the framework of Increase Competitiveness Program of NUST «MISiS» (№ К3-2018-030), implemented by a governmental decree dated 16th of March 2013, N 211. This work was supported in part by the European Social Fund's Doctoral Studies and Internationalisation Programme DoRa and Estonian Research Council (PUT1081); in part by M.V. Lomonosov Moscow State University Program of Development.

References

[1] P.-A. Douissard, A. Cecilia, T. Martin, V. Chevalier, M. Couchaud, T. Baumbach, K. Dupre, M. Kuehbacher, A. Rack, A novel epitaxially grown LSO-based thin-film scintillator for micro-imaging using hard synchrotron radiation, J. Synchrotron Radiat. 17 (2010) 571–583, https://doi.org/10.1107/S0909049510025938.

[2] M.S. Alekhin, J. Renger, M. Kasperczyk, P.-A. Douissard, T. Martin, Y. Zorenko, D.A. Vasil'ev, M. Stiefel, L. Novotny, M. Stampanoni, STED properties of Ce^{3+}, Tb^{3+}, and Eu^{3+} doped inorganic scintillators, OPT EXPRESS 25 (2017) 1251–1261, https://doi.org/10.1364/OE.25.001251.

[3] M.S. Alekhin, G. Patton, C. Dujardin, P.-A. Douissard, M. Lebugle, L. Novotny, M. Stampanoni, Stimulated scintillation emission depletion X-ray imaging, OPT EXPRESS 25 (2017) 654–669, https://doi.org/10.1364/OE.25.000654.

[4] J. Bok, O. Lalinský, M. Hanuš, Z. Onderišinová, J. Kelar, M. Kučera, GAGG:ce single crystalline films: new perspective scintillators for electron detection in SEM, Ultramicroscopy 163 (2016) 1–5, https://doi.org/10.1016/j.ultramic.2016.01.003.

[5] K. Kamada, T. Endo, K. Tsutumi, T. Yanagida, Y. Fujimoto, A. Fukabori, A. Yoshikawa, J. Pejchal, M. Nikl, Composition engineering in cerium-doped $(Lu,Gd)_3(Ga,Al)_5O_{12}$ single-crystal scintillators, Cryst. Growth Des. 11 (2011) 4484–4490, https://doi.org/10.1021/cg200694a.

[6] Y. Wu, F. Meng, Q. Li, M. Koschan, Ch.L. Melcher, Role of Ce^{4+} in the scintillation mechanism of codoped $Gd_3Ga_3Al_2O_{12}$:Ce, Phys Rev Appl 2 (2014) 44009, https://doi.org/10.1103/PhysRevApplied.2.044009.

[7] M. Tyagi, F. Meng, M. Koschan, S.B. Donnald, H. Rothfuss, Ch.L. Melcher, Effect of codoping on scintillation and optical properties of a Ce-doped $Gd_3Ga_3Al_2O_{12}$ scintillator, J. Phys. D Appl. Phys. 46 (2013) 475302, https://doi.org/10.1088/0022-3727/46/47/475302.

[8] K. Kamada, M. Nikl, Sh. Kurosawa, A. Beitlerova, A. Nagura, Y. Shoji, J. Pejchal, Y. Ohashi, Y. Yokota, A. Yoshikawa, Alkali earth co-doping effects on luminescence and scintillation properties of Ce doped $Gd_3Al_2Ga_3O_{12}$ scintillator, Opt. Mater. 41 (2015) 63–66, https://doi.org/10.1016/j.optmat.2014.10.008.

[9] Q. Meng, Ji-G. Li, Q. Zhu, X. Li, X. Sun, The effects of Mg^{2+}/Si^{4+} substitution on crystal structure, local coordination and photoluminescence of $(Gd,Lu)_3Al_5O_{12}$:Ce garnet phosphor, J Alloy Compd 797 (2019) 477–485, https://doi.org/10.1016/j.jallcom.2019.05.086.

[10] N.V. Vasil'eva, V.V. Randoshkin, V.G. Plotnichenko, Yu.N. Pyrkov, V.V. Voronov, A.M. Galstyan, N.N. Sysoev, Effect of Pb ions on the optical absorption in $Gd_3Ga_5O_{12}$ epitaxial films, Inorg Mater 44 (2008) 76–81, https://doi.org/10.1134/S0020168508010135.

[11] I.I. Syvorotka, D. Yu. Sugak, A.P. Luchechko, Ya.A. Zhydachevskyy, S.B. Ubizskii, Optical properties of GGG epitaxial films grown from $PbO–B_2O_3–V_2O_5$ flux, Acta Phys. Pol., A 133 (2018) 954–958, https://doi.org/10.12693/APhysPolA.133.954.

[12] N.V. Vasil'eva, V.V. Randoshkin, V.G. Plotnichenko, Yu.N. Pyrkov, V.V. Koltashev, A.M. Galstyan, N.N. Sysoev, Epitaxial films $(Bi,Gd)_3(Ga,Pt)_2Ga_3O_{12}$ grown by liquid-phase epitaxy, J Surf Invest-X-ray 2 (2008) 48–51, https://doi.org/10.1007/s11700-008-1008-y.

[13] A.P. Luchechko, I.I. Syvorotka, Y. Zakharko, I.M. Syvorotka, Growing features and luminescence of Bi^{3+} ions in $Gd_3Ga_5O_{12}$ epitaxial films, Solid State Phenom. 200 (2013) 215–219, https://doi.org/10.4028/www.scientific.net/SSP.200.215.

[14] A. Krasnikov, A. Luchechko, E. Mihokova, M. Nikl, I.I. Syvorotka, S. Zazubovich, Ya. Zhydachevskii, Origin of Bi^{3+}–related luminescence in $Gd_3Ga_5O_{12}$:Bi epitaxial films, J. Lumin. 19 (2017) 81–88, https://doi.org/10.1016/j.jlumin.2017.05.050.

[15] M. Nikl, A. Yoshikawa, Recent R&D trends in inorganic single-crystal scintillator materials for radiation detection, Opt. Mater. 3 (2015) 463–481, https://doi.org/10.1002/adom.201400571.

[16] T. Karner, V.V. Laguta, M. Nikl, T. Shalapska, S. Zazubovich, On the origin of cerium-related centres in lead-containing single crystalline films of Y_2SiO_5 :Ce and Lu_2SiO_5 :Ce, J. Phys. D Appl. Phys. 47 (2014), https://doi.org/10.1088/0022-3727/47/6/065303, 065303(7pp).

[17] S.I. Omelkov, V. Nagirnyi, A.N. Vasil'ev, M. Kirm, New features of hot intraband luminescence for fast timing, J. Lumin. 176 (2016) 309–317, https://doi.org/10.1016/j.jlumin.2016.03.039.

[18] G.B. Scott, J.L. Page, Pb valence in iron garnets, J. Appl. Phys. 48 (1977) 1342–1349, https://doi.org/10.1063/1.323728.

[19] J.M. Ogiegło, A. Katelnikovas, A. Zych, Th. Justel, A. Meijerink, C.R. Ronda, Luminescence and luminescence quenching in $Gd_3(Ga,Al)_5O_{12}$ scintillators doped with Ce^{3+}, J. Phys. Chem. 11 (2013) 72479–72484, https://doi.org/10.1021/jp309572p.

[20] V.V. Randoshkin, N.V. Vasil'eva, V.G. Plotnichenko, Yu.N. Pyrkov, S.V. Lavrishchev, M.A. Ivanov, A.A. Kiryukhin, A.M. Saletski, N.N. Sysoev, Optical absorption by Nd^{3+} and Gd^{3+} ions in epitaxial films grown on $Gd_3Ga_5O_{12}$substrates from a lead-containing solution melt, Phys. Solid State 46 (2004) 1030–1036, https://doi.org/10.1134/1.1767239.

[21] R.W. Gurney, N.F. Mott, Luminescence in solids, T Faraday Soc 35 (1939) 69–73, https://doi.org/10.1039/TF9393500069.

[22] J. Ueda, P. Dorenbos, A.J.J. Bos, A. Meijerink, S. Tanabe, Insight into the thermal quenching mechanism for $Y_3Al_5O_{12}:Ce^{3+}$ through thermoluminescence excitation spectroscopy, J. Phys. Chem. C 119 (2015) 25003–25008, https://doi.org/10.1021/acs.jpcc.5b08828.

[23] S.I. Omelkov, V. Nagirnyi, S. Gundacker, D.A. Spassky, E. Auffray, P. Lecoq, M. Kirm, Scintillation yield of hot intraband luminescence, J. Lumin. 198 (2018) 260–271, https://doi.org/10.1016/j.jlumin.2018.02.027.

[24] R.M. Turtos, S. Gundacker, M. Pizzichemi, A. Ghezzi, K. Pauwels, E. Auffray, P. Lecoq, M. Paganoni, Measurement of LYSO intrinsic light yield using electron excitation, IEEE Trans. Nucl. Sci. 63 (2016) 475–479, https://doi.org/10.1109/TNS.2016.2527738.

[25] E. Auffray, S. Baccaro, T. Beckers, Y. Benhammou, A.N. Belsky, B. Borgia, D. Boutet, R. Chipaux, I. Dafinei, F. de Notaristefani, P. Depasse, C. Dujardin, H.E. Mamouni, J.L. Faure, J. Fay, M. Goyot, S.K. Gupta, A. Gurtu, H. Hillemanns, B. Ille, T. Kirn, M. Lebeau, P. Lebrun, P. Lecoq, J.A. Mares, J.P. Martin, V.V. Mikhailin, B. Moine, J. Nelissen, M. Nikl, C. Pedrini, R. Raghavan, Extensive studies on CeF_3 crystals, a good candidate for electromagnetic calorimetry at future accelerators, Nucl Instrum Meth A 383 (1996) 367–390, https://doi.org/10.1016/S0168-9002(96)00806-6.

[26] I.V. Khodyuk, P. Dorenbos, Trends and patterns of scintillator nonproportionality, IEEE Trans. Nucl. Sci. 59 (2012) 3320–3331, https://doi.org/10.1109/TNS.2012.2221094.

[27] W. Klamra, P. Sibczynski, M. Moszynski, W. Czarnacki, V. Kozlov, Extensive studies on light yield non-proportional response of undoped CeF_3 at room and liquid nitrogen temperatures, J. Instrum. 8 (2013) 6003, https://doi.org/10.1088/1748-0221/8/06/P06003.

[28] P. Sibczynski, J. Iwanowska-Hanke, M. Moszyński, L. Swiderski, M. Szawłowski, M. Grodzicka, T. Szczęśniak, K. Kamada, A. Yoshikawa, Characterization of GAGG:Ce scintillators with various Al-to-Ga ratio, Nucl. Instrum. Meth. A 772 (2015) 112–117, https://doi.org/10.1016/j.nima.2014.10.041.

[29] B.L. Henke, E.M. Gullikson, J.C. Davis, X-ray interactions: photoabsorption, scattering, transmission, and reflection at E=50-30000 eV, Z=1-92, Atom Data Nucl. Data 54 (1993) 181–342, https://doi.org/10.1006/adnd.1993.1013.

[30] M. Kirm, A. Andrejczuk, J. Krzywinski, R. Sobierajski, Influence of excitation density on luminescence decay in $Y_3Al_5O_{12}$:Ce and BaF_2 crystals excited by free electron laser radiation in VUV, Phys. Status Solidi C 2 (2005) 649–652, https://doi.org/10.1002/pssc.200460255.

[31] W.W. Moses, G.A. Bizarri, R.T. Williams, S.A. Payne, A.N. Vasil'ev, J. Singh, Q. Li, J.Q. Grim, W.-S. Choong, The origins of scintillator non-proportionality, IEEE Trans. Nucl. Sci. 59 (2012) 2038–2044, https://doi.org/10.1109/TNS.2012.2186463.

[32] G. Tamulaitis, A. Vasil'ev, M. Korzhik, A. Mazzi, A. Gola, S. Nargelas, A. Vaitkevicius, A. Fedorov, D. Kozlov, Improvement of the time resolution of radiation detectors based on $Gd_3Al_2Ga_3O_{12}$ scintillators with SiPM readout, IEEE Trans. Nucl. Sci. 66 (2019) 1879–1888, https://doi.org/10.1109/TNS.2019.2919898.

[33] Sh. Liu, X. Feng, Zh. Zhou, M. Nikl, Yu. Shi, Yu. Pan, Effect of Mg^{2+} co-doping on the scintillation performance of LuAG:Ce ceramics, Phys Status Solidi-R. 8 (2014) 105–109, https://doi.org/10.1002/pssr.201308199.

[34] S. Blahuta, A. Bessière, B. Viana, P. Dorenbos, V. Ouspenski, Evidence and consequences of Ce in LYSO:Ce,Ca and LYSO:Ce,Mg single crystals, IEEE Trans. Nucl. Sci. 60 (2013) 3134–3141, https://doi.org/10.1109/TNS.2013.2269700.